Electronic structure of defects and impurities in III-V nitrides. II. Be, Mg, and Si in cubic boron nitride

V. A. Gubanov and E. A. Pentaleri
Physics Department, San Jose State University, San Jose, California 95192-0106

C. Y. Fong and B. M. Klein
Department of Physics, University of California, Davis, California 95616-8677

(Received 30 August 1996; revised manuscript received 11 August 1997)

The electronic structure of beryllium (Be), magnesium (Mg), and silicon (Si) impurities in zinc-blende boron nitride (c-BN) were studied by using the tight-binding linearized muffin-tin-orbitals technique. Calculations were performed using 64-atom supercells centered on either a boron (B) or a nitrogen (N) lattice site. While Be and Mg impurities were substituted only to the B sublattice, substitutions for both B and N were considered in the case of the Si impurity. In each case, total-energy minimization was used to examine lattice relaxation near the impurity site, and the nature of chemical bonding between the impurity and the neighboring atoms of the host crystal was examined in detail. We find that Be and Mg substituted for B each create delocalized levels merged to the states at the valence-band edge. These partially occupied levels can result in p-type conductivity such as that which has been observed experimentally. In contrast to the behavior of isolated Be and Mg impurities in c-BN, we find that Si substituted at a B site induces delocalized impurity states that overlap with the conduction-band edge of the host. These levels can contribute to the n-type conductivity of Si-doped c-BN. Si substituted to the anion sublattice induces sharp, partially occupied, and highly localized levels within the forbidden gap (''deep acceptor levels''). The experimentally observed mixture of n- and p-type c-BN can therefore be accounted for by the presence of impurities of each type. The relaxation of the host lattice near the Be and Mg impurities is outward, as is the relaxation near the Si impurity substituted at a N site. Inward relaxation is predicted in the case of Si substituted for B. The total, orbital, and shell-projected densities of states for the impurity and up to six coordinational shells nearest the impurity are analyzed in detail. Charge-density plots relevant to the impurities are also presented.
[S0163-1829(97)01244-7]

I. INTRODUCTION

It has been recognized for more than two decades that the development of radiation-resistant high-power and high-temperature microelectronic devices may well be possible by using ''wide-gap semiconductors,'' such as diamond (C), cubic silicon carbide (c-SiC) and III-V nitrides. These crystals have forbidden gaps ranging from 2.3 eV in c-SiC, to 6.4 eV in boron nitride (BN).[1,2] Combined with their remarkable thermomechanical properties, these materials provide exciting opportunities for fabricating devices with operating characteristics superior to those made of pure Si and germanium.

Two factors have inhibited the practical use of these materials in microelectronics, however: (1) the absence of reliable, well-controlled thin-film-deposition techniques for providing stable single-phase epitaxial layers of ''semiconductor purity'' and good adhesion to a variety of substrates, and (2) the need for reliable methods for selective doping. Substantial progress has recently been made in thin-film-deposition techniques for BN, with the demonstration that even under extreme conditions a metastable zinc-blende BN (c-BN) phase can be formed[3–5] on several substrates relevant to microelectronics applications, particularly Si(001).[6,7] Furthermore, c-BN has been shown to be easily doped with both n- and p-type impurities. Mishima *et al.*,[8] used Si to obtain n-type semiconducting materials, while Be-doped samples have demonstrated p-type behavior. In each case, the ionization energies were found to be very low. Near room temperature, activation of impurity-related carriers to the continuum has been readily observed. Diodes fabricated from these materials demonstrated a broad emission spectrum of ultraviolet and visible radiations.[9] Active research with such systems is under way in several laboratories.[5,7,10]

While these developments are encouraging, many materials-science issues remain to be understood. Important physics relevant to improved device operation and future developments for electronic materials are still needed. What is the microscopic origin of the n- and p-type conductivities in doped systems, for example? How are electronic states affected by charge transfer or by the chemical bonding in doped crystals? What are the effects of lattice relaxation near impurity sites on the doping effectiveness? Understanding these basic questions is especially important for c-BN, for which presently available experimental information focuses exclusively on deposition techniques and techniques for chemical and structural characterization. (See, for example, Refs. 11 and 12.) Extensive theoretical modeling of the electronic structure has been limited mainly to ideal, stoichiometric c-BN crystals.[13–15]

This paper is a continuation of our efforts to apply the supercell band-structure technique to the investigation of electronic structure and chemical bonding in c-BN crystals

containing defects and impurities. In the first paper of this series,[16] we studied boron (B) and nitrogen (N) vacancies in nonstoichiometric *c*-BN. We now examine the electronic structure of *n*- and *p*-doped *c*-BN. The paper is organized as follows: In Sec. II, the theoretical model and technical details of the calculations are reviewed briefly. The results of supercell calculations for *p*-type beryllium (Be) and magnesium (Mg) impurities in *c*-BN are presented in Sec. III. In Sec. IV, we discuss the electronic structure of Si-doped *c*-BN for both cation- and anion-type substitutional impurities. The calculations and results are summarized in Sec. V.

II. MODEL AND CALCULATIONAL TECHNIQUE

The electronic structures of Be-, Mg-, and Si-doped *c*-BN were calculated by using the same supercell model as described previously[16] to investigate B and N vacancies in *c*-BN. The *c*-BN lattice parameter is taken to be 3.615 Å.[17]

As discussed previously, we used the tight-binding linearized muffin-tin-orbitals technique without empty spheres (TB-LMTO-no-ES) within the local-density approximation (LDA) for calculating the properties of nonstoichiometric and doped *c*-BN. To validate the use of this model, benchmark calculations were performed for stoichiometric *c*-BN crystals to compare results obtained using the full-potential linearized augmented plane-wave (FPLAPW) technique[18] and the full-potential linearized muffin-tin-orbitals (FPLMTO) technique[19] with those obtained from the computationally more efficient TB-LMTO-no-ES technique. Sensitivity of the results to a number of input parameters (muffin-tin and atomic-sphere radii, the introduction of empty spheres into the LMTO-based models, etc. was carefully analyzed.[16] These comparisons showed that the FPLAPW, FPLMTO, and TB-LMTO-no-ES (Ref. 20) techniques provide consistent and practically identical predictions of the electronic structure of stoichiometric *c*-BN, except for energy regions far above the conduction-band edge, where higher-energy conduction-band states are sensitive to the input parameters and the particular computational techniques used.[16] The 4.4-eV predicted band gap between occupied and empty levels is significantly smaller than the experimentally observed value of 6.0–6.4 eV, this underestimate being well known and common to all of the LDA calculations. The calculated band gap can, of course, be significantly improved by using the computationally intensive *GW* method,[21] or even by using simple parametrized approaches, as suggested by Bernstedt and Del Sole.[22] *GW* and similar techniques, however, become prohibitively time consuming when they are applied to complex systems such as the supercells that must be used to describe isolated vacancies and impurities. In the present paper, therefore, we have limited ourselves to LDA-type calculations.

To ensure that the LMTO-TB-no-ES technique yields reliable results when it is applied to impurity supercells, we reproduce in Fig. 1 the total and partial densities of states (DOS) for ideal *c*-BN, which are in agreement with the results of FPLAPW calculations shown in Ref. 16. Several features of Fig. 1 should be noted. The lowest portion of the valence band is composed mainly of N 2*s* states, with some covalent admixtures of B 2*p* states, and an even smaller contribution due to B 2*s* states. This part of the valence band

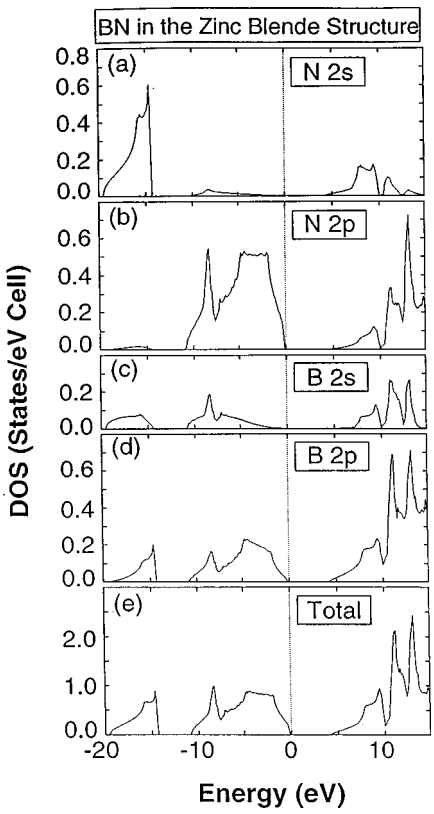

FIG. 1. Total and partial densities of states for an ideal *c*-BN crystal.

is split off from the upper part of the valence band by an energy difference of about 3 eV, due to the effect of the strong N ion potential on its own *s*-like states. The high ionicity of the N atom also affects the *s*- and *p*-like states of the B atom. The upper portion of the valence band consists predominantly of N 2*p* states, with significant contributions of B 2*s* and B 2*p* states. These are the typical features of the more ionic III-V compounds. The states at the valence-band edge originate completely from N 2*p* states. The low-energy conduction bands are mixtures of comparable contributions from all antibonding B 2*s* states with a somewhat larger contribution of B 2*p* states at the conduction-band edge.

To model an isolated impurity in *c*-BN, we used a model similar to that used previously to represent isolated B and N vacancies: a primitive cubic supercell consisting of eight cubic cells in the zinc-blende structure. In each case, the impurity atom was substituted at the center of the 64-atom supercell, yielding an effective impurity concentration of 1.56%.

The band-structure calculations were performed in the basis of the *s*, *p*, and *d* states of the B, N, and impurity atoms. The Hedin-Lundqvist exchange-correlation potential[23] was used. Ten special **k**-space points in the irreducible part of the Brillouin zone were used in the calculations. The ratios of the atomic sphere radii for B, N, and impurity atoms were chosen from the construction of overlapping atomic Hartree potentials for the doped crystals. The calculated energy levels and densities of states were found to be rather insensitive to variation (in the range of 10–15 %) about the sphere radii that were used in the calculations, however. Though the charge localized inside the atomic spheres did, indeed, vary as the atomic-sphere radii were changed, the qualitative fea-

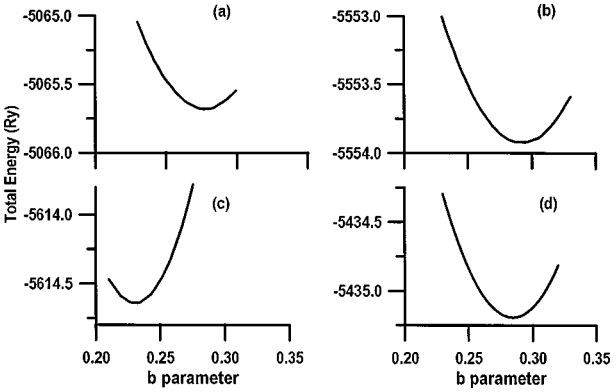

FIG. 2. Total energy of doped c-BN supercells as a function of the bond-length parameter, b. (a) Be impurity at a B site. (b) Mg impurity at a B site. (c) Si at a B site. (d) Si at a N site.

tures of charge transfer (the direction of charge transfer, and the impurity perturbations relative to undoped crystals) were unchanged by adjusting the ratios of atomic-sphere radii. The calculations were performed on a CRAY C-90 using the computer code developed by van Schilfgaarde *et al.*[24]

To evaluate the delocalization of the impurity states, we allowed the atoms in each of the coordinational shells surrounding the impurity site to adjust their eigenstates and corresponding charge distributions. By independently varying the charge distribution and potential for each coordinational shell (the atoms nearest the impurity forming the first shell, the second-nearest neighbors constituting the second shell, and so forth), the extent of delocalization was determined by inspecting the local DOS corresponding to each shell (the ''shell-projected'' DOS).

Because the ''sizes'' of the impurity atoms differ from those of the host crystal, such substitutional impurities can introduce localized distortions to the host lattice. We investigated such distortions by allowing the first shell of atoms to relax with respect to the impurity site, while maintaining the tetragonal symmetry of the zinc-blende structure. The total-energy calculations were performed for various positions of the atoms nearest to the impurity site, and the equilibrium bond lengths were determined from the minimum of the total energy. No attempts were made to consider asymmetric distortions of the neighboring atoms. Furthermore, due to the large number of atoms in the supercell, force calculations necessary to estimate the relaxation of more distant atoms are prohibitive within our available resources, and were therefore not performed.

III. Be AND Mg IMPURITIES IN c-BN

The electronic structures of Be- and Mg-doped c-BN were calculated by using 64-atom supercells with the central B atom replaced by an impurity atom. In Fig. 2, we present the total-energy variation of c-BN:Be and c-BN:Mg as a function of the bond length between the impurity and its nearest-neighbor N atoms. It is convenient to describe the bond-length change in terms of the quantity b, defined as the ratio of the distance between the impurity atom and its nearest neighbors to the lattice constant of the zinc-blende structure. In each case, introducing the impurity results in a significant outward relaxation relative to the nominal value of b in the undistorted lattice: 0.25. The predicted equilibrium value of b is 0.278 in the case of the Be impurity, and 0.286 for Mg. These values correspond to an increase of the Be-N and Mg-N bond lengths to 1.74 and 1.79 Å, respectively, as compared with the 1.57-Å value between B and N atoms in the c-BN host crystal. This large outward relaxation cannot be accounted for on the simple basis of ''size,'' as a Be atom has a smaller atomic radius than that of the B atom for which it substitutes.

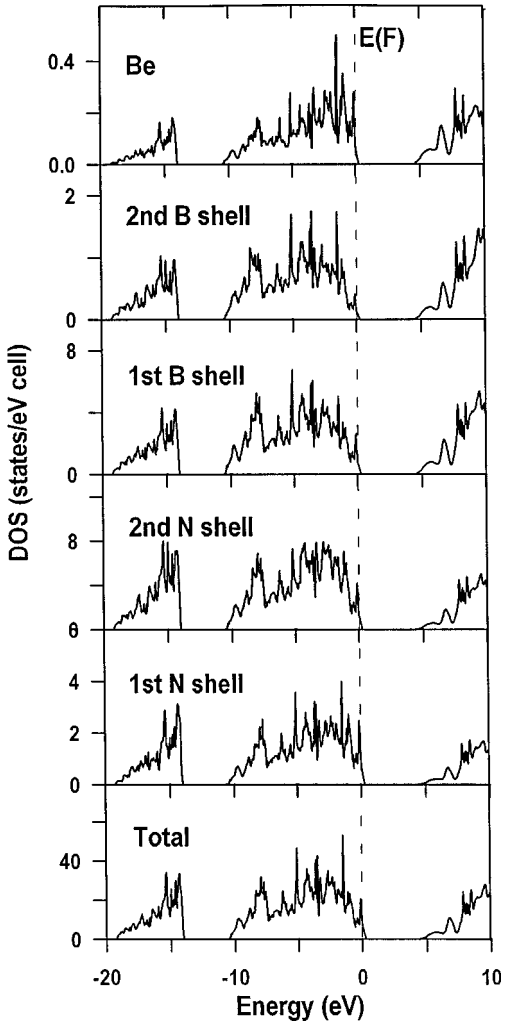

FIG. 3. Total and shell-projected densities of states for a Be impurity at a B site in BN.

Because the Be atom has one less valence electron than the B atom, the Be-N bonds are not as strong as the N-atom bonds with their neighboring B atoms. The reduction of this bond strength may therefore account for the predicted outward relaxation. A similar mechanism should apply to the Mg impurity. In addition, the Mg atom is larger than the B atom, so that an additional outward relaxation may be expected in this case, consistent with the observed predictions.

The total and shell-projected DOS for atoms up to the fourth-nearest neighbors of the Be atom is shown in Fig. 3. The upper panel shows the total DOS for the impurity atom. Both Be $2s$ and Be $2p$ states overlap the entire valence band of the host crystal, the distribution being rather uniform, with relatively stronger contributions being made near the valence-band edge. The most important feature of the DOS

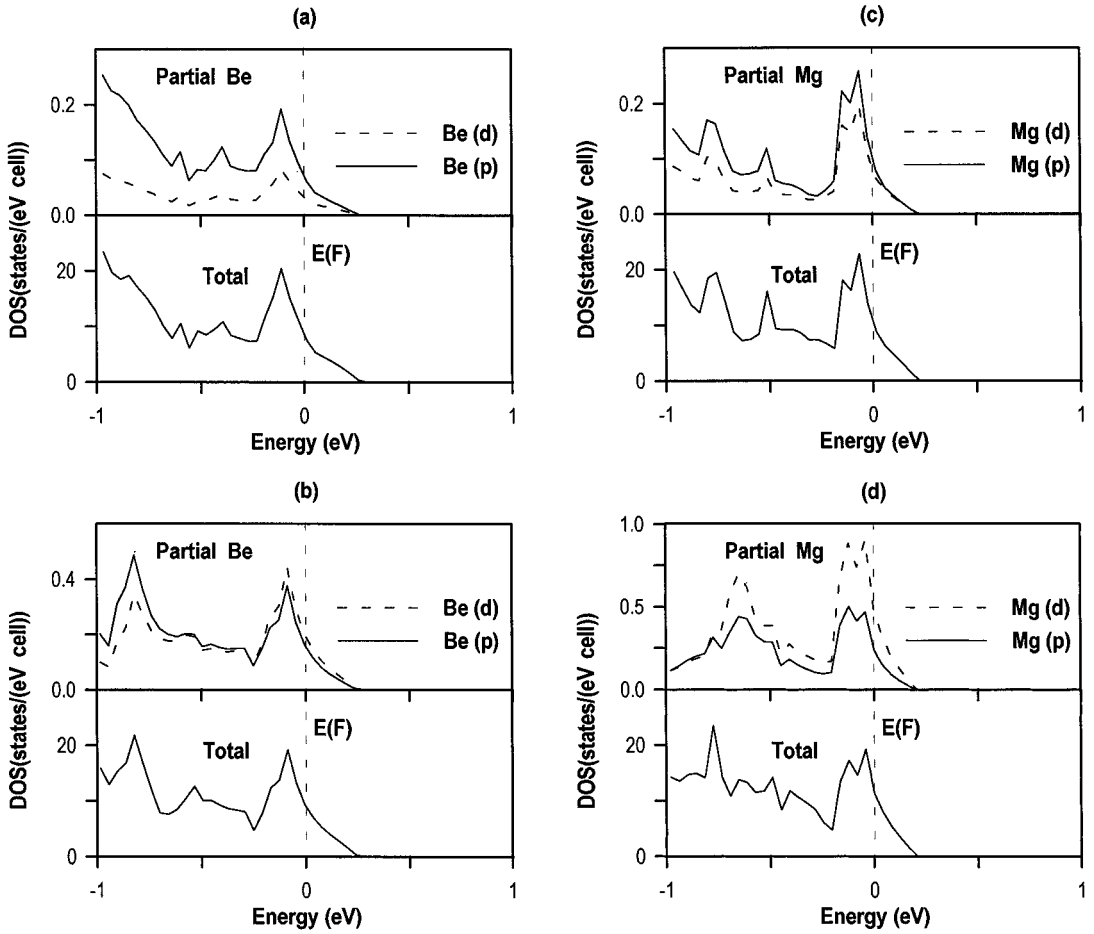

FIG. 4. p and d orbital-projected densities of states for (a) relaxed and (b) unrelaxed configurations of the lattice surrounding the Be impurity, and (c) relaxed and (d) unrelaxed configurations of the lattice surrounding the Mg impurity.

for the c-BN:Be system is, indeed, the position of the Fermi level. With one fewer electron in Be than in the B atom it replaces, the Fermi level falls within the valence band, the resulting empty states being responsible for the experimentally observed p-type conductivity.[8] The traditional model of localized, shallow acceptor levels split off from the valence-band edge does not appear to be applicable to the Be impurity in c-BN. Unlike ideal c-BN, both B and N atoms as far as the third coordinational shells contribute significantly to the valence-band DOS. The impurity increases the bonding of these atoms at the same time that bonding to the impurity site is reduced. This is the origin of the outward relaxation discussed above.

The hole states induced by the Be impurity at the valence-band edge have substantial contributions from the impurity atom and its neighbors. The hole states are therefore highly delocalized in the crystal, and may therefore contribute high-mobility p-type carriers.

Figure 4 shows the structure of the Be states near the Fermi level. As expected, the major contribution to the band-edge DOS is from the Be $2p$ states. The relaxation of the crystal lattice near the impurity significantly reduces the Be $2p$ contributions to the states of the valence-band edge [Fig. 4(a)], as compared with the unrelaxed configuration [Fig. 4(b)]. The DOS at the Fermi level (Table I) decreases from 8.96 states/(eV cell) to 8.62 states/(eV cell) for the relaxed configuration, with a corresponding lowering of the Fermi level by 0.02 eV with respect to the value of the unrelaxed case of -2.80 eV.

Figure 5 shows charge-density plots in the (110) plane for states with energies near the Fermi level (Fig. 3), and the total charge densities in the (110) and (100) planes [Figs. 5(b) and 5(c)] containing the Be atom. Even with the nearest-neighbor atoms relaxed, there is not much charge at the Be atom, as shown in the total charge-density maps. A *qualitative* picture for the hole states can be obtained from Fig. 5(a).

TABLE I. The densities of states at the Fermi level, N(E_F), and Fermi energies in doped c-BN crystals: LMTO-TB calculation results for $Be_{0.015}B_{0.985}N$(I), $Mg_{0.015}B_{0.985}N$(II), $Si_{0.015}B_{0.985}N$(III), and $Si_{0.015}BN_{0.985}$(IV).

Parameter	Be at B site (I)	Mg at B site (II)	Si at B site (III)	Si at N site (IV)
Fermi energy (eV):				
unrelaxed crystal	−2.80	−2.68	2.41	1.01
relaxed crystal	−2.82	−2.57	2.42	0.81
DOS at E_F: (states/eV cell)				
unrelaxed crystal	8.96	11.6	2.80	38.0
relaxed crystal	8.62	10.7	2.80	40.0

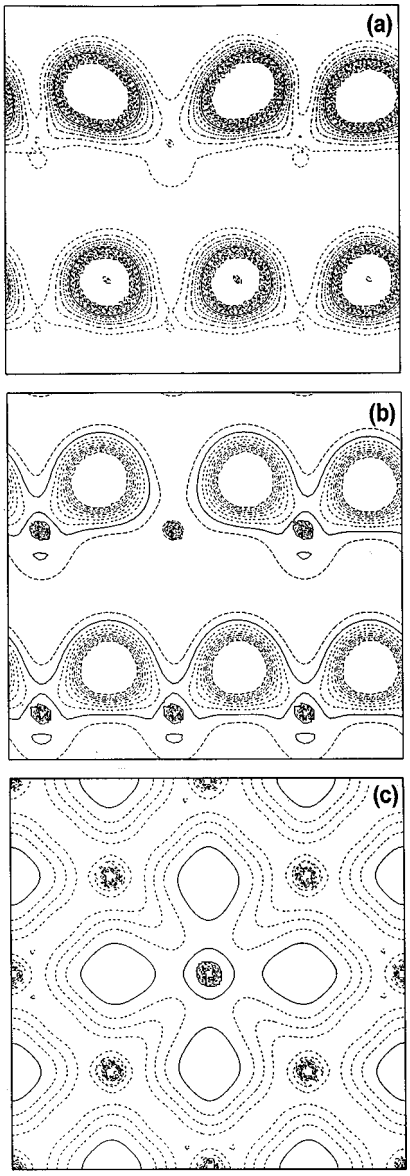

FIG. 5. Charge-density maps for a crystal with an isolated Be impurity substituted at a B site. (a) (110)-plane charge density for hybridized states near the Fermi level. (b) (110)-plane total valence charge density. (c) (100)-plane total valence charge density.

The charge densities associated with the hole states are highly delocalized over many coordinational spheres, with dominant contributions from the states of the N atoms. A relatively larger contribution is made by the Be states than by the states of the B atoms.

The charge transfer between the Be atom and its neighboring atoms can be estimated from the values of the charges within the atomic spheres. These show that the Be impurity loses considerably more electronic charge than the B atoms, so its effective ionic charge is larger than that of the B atoms. The electronic charge lost by the Be atom is transferred mostly to the nearest N atoms. Such charge transfer is not limited to the atoms of the first N shell, however. The charge densities within the atomic spheres of up to the third B and N shells are affected. These are the so-called ''back bonds.'' Our calculations suggest that the 64-atom supercell is sufficiently large as to ensure the effective isolation of the Be impurity.

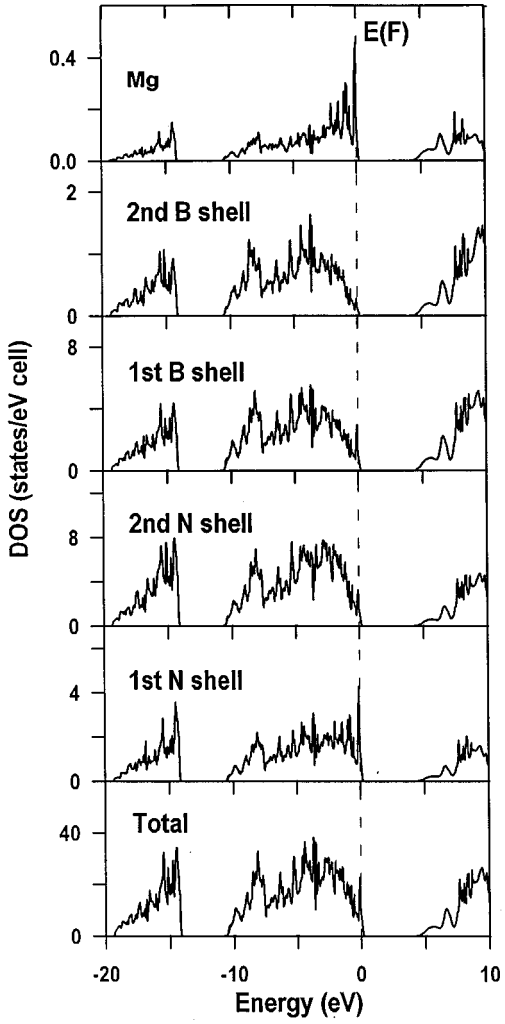

FIG. 6. Total and shell-projected densities of states for a Mg impurity at a B site in c-BN.

The TB-LMTO-no-ES calculations discussed above suggest that Be substitutional impurities can readily create hole states near the top of the valence band, which can result in p-type conductivity in c-BN:Be. This result agrees with experimental observations.[8] In contrast to the traditional impurity doping model, the impurity-related states are strongly delocalized, and cannot be described as narrow ''impurity acceptor levels'' located at the top of the valence band of the ideal crystal.

The other candidate frequently considered for creating p-type conductivity in III-V nitrides is Mg.[1,2] The results of calculations performed for this impurity are presented in Figs. 6 and 7 and Table I. Unless noted otherwise, the results pertain to the configuration in which the nearest neighbors to the impurity have been radially relaxed to their equilibrium position, as determined by minimizing total energy with respect to the radial coordinate.

The total DOS obtained for the c-BN:Mg system (Fig. 6) is rather similar to the c-BN:Be case. Mg $3s$ and $3p$ states make prominent contributions to the entire valence band (we also include the d states of Mg in the calculations). Their distribution, however, is much less uniform than in the case of the Be impurity (Fig. 3). The atomic energy of the $3p$ states for the Mg atom is significantly higher than that of the

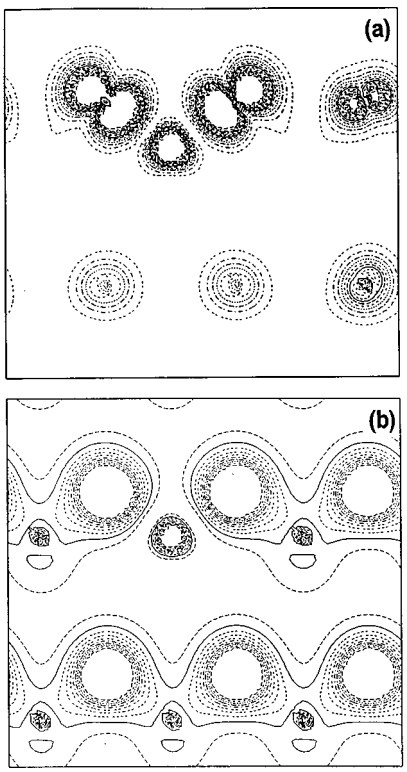

FIG. 7. Charge-density maps for a c-BN crystal with an isolated Mg impurity at a B site. (a) (110)-plane charge density in hybridized states near the Fermi level. (b) (110)-plane total valence-band charge density.

Be $2p$ states. Consequently, Mg $3p$ states appear near the valence-band edge (the upper panel in Fig. 6) with a narrow, sharp peak showing their strong localization. As in the case of the Be impurity, the Fermi level passes through the upper part of the sharp peak. Empty states appear in the valence band, and p-type conductivity appears to be possible in c-BN:Mg. The shell-projected DOS (not shown) indicates a strong interaction between the Mg $3p$ states and the $2p$ states of the neighboring N atoms (the first N shell). The features of the Mg impurity are more localized than the corresponding features of the Be impurity, with the dominant peaks in the Mg and first-N-shell partial DOS twice the amplitude of those that appear in the case of the Be-impurity partial DOS. The DOS at the Fermi level, $N(E_F)$, for Mg-doped c-BN is larger than for the c-BN:Be system (Table I). Lattice relaxation near the impurity site decreases $N(E_F)$ from 11.6 states/(eV cell) in the unrelaxed calculations to 10.7 states/(eV cell) in the relaxed case, with a corresponding *down*shift of E_F by 0.1 eV.

In Figs. 4(c) and 4(d), we expand the DOS near the Fermi level for the relaxed [Fig. 4(c)] and unrelaxed [Fig. 4(d)] host crystal. As in the case of the Be-doped crystal, the Mg p states dominate the band structure near the Fermi level. The participation of the Mg s states is virtually negligible in comparison. In contrast to the case of the Be impurity, the strong relaxation of the atoms neighboring the Mg impurity and the corresponding distortion of the electronic charge-density distribution near the Mg atom may very well require the introduction of the Mg d orbitals in order to obtain an accurate description of the states near the top of the valence band in c-BN:Mg.

Examining the charge transfer between atomic spheres, it was found that the Mg atom is much more easily ionized than the Be atom. About one electron is depleted from the Mg atomic sphere. It is transferred mainly to the atoms of the first N shell, and, to a lesser extent, to the atoms of the first B shell. This effect is also evident in the (110)-plane distribution of charges in an energy band near the Fermi level, shown in Fig. 7(a), and in the total-charge-density distribution shown in Fig. 7(b). The ionic bonding between the impurity and its neighboring N atoms is clearly shown in Fig. 7(a), with the charges being localized about the impurity and its nearest neighbors. The strong p-like character of the states is clearly manifested at the N atoms of the first coordinational shell. The states that remain associated with the Mg atom show a distorted s-like character (mixed with d-type characteristics), and contribute to states near the Fermi level. The presence of the Mg impurity, however, significantly deforms the distribution of charges near the Fermi level that are associated with the atoms of the first N shell, as is evident by comparing the charge-density contours for the upper chain (which includes the impurity) to those of the lower chain (which has no impurity) in Fig. 7(b). The role of the Mg impurity in forming the hole state in the valence band appears to be more localized, mainly by distorting sp^3-type states of the first-N-shell atoms away from the impurity site. This is in contrast to the results observed for the Be-impurity calculations, in which states near the Fermi level were found to be rather delocalized and to participate with N $2p$ states in hole-state formation.

The TB-LMTO supercell calculations show that both Be and Mg impurities in the c-BN crystal behave as acceptorlike impurities, and induce hole states at the valence-band edge, which can result in p-type conductivity. Our results are consistent with experimental observations that Be-doped c-BN exhibits p-type transport properties.[8] The impurity valence states overlap strongly with the host valence band. The model of a narrow, isolated acceptor impurity level split off from the valence-band edge is not applicable. On the other hand, the character of the hole states for the two impurities are rather different from one another. In contrast to the more localized states induced by the Mg impurity, the Be atom forms highly delocalized hole states in the vicinity of the Fermi level, which may explain the high mobility of holes that has been shown in experimental data.

IV. Si IMPURITIES IN c-BN

BN has been successfully doped with Si, exhibiting n-type conductivity.[8,9] The experimental data available for Si-doped BN, however, are very scarce.

We applied the TB-LMTO-no-ES technique to investigate the electronic properties of isolated Si impurities replacing either a cation or an anion in c-BN. As was done for the Be- and Mg-impurity calculations, the atoms nearest the impurity were relaxed by minimizing total energy with respect to the radial distance from the impurity site. An inward relaxation is predicted when a Si atom replaces B, with the minimum of total energy occurring at the b-parameter coordinate of 0.23. The corresponding length of the Si-N bonds is 1.44 Å. In the case of a Si atom substituted at a N site, outward relaxation was predicted. In this case, the total-energy minimum oc-

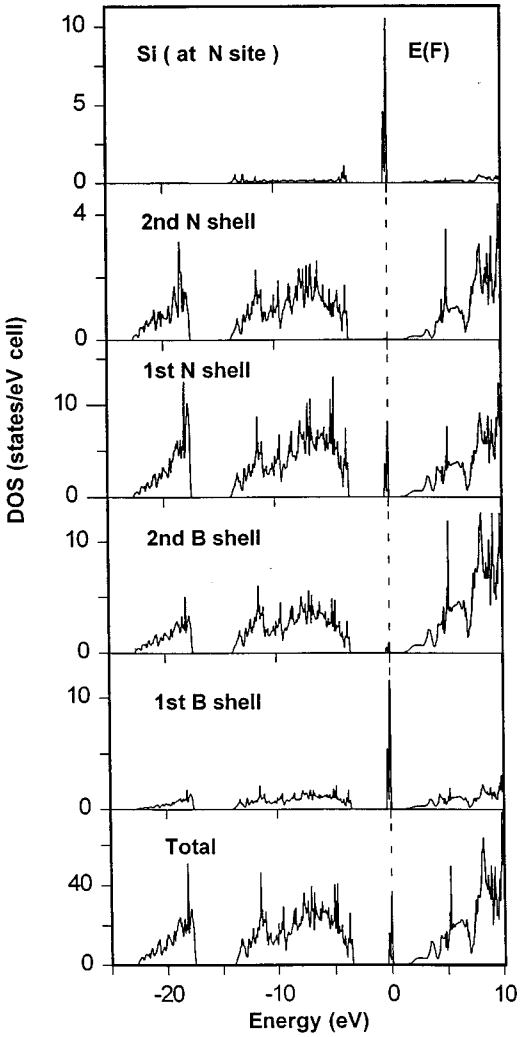

FIG. 8. Total and shell-projected DOS for an isolated Si impurity at a N site in c-BN: Si impurity, second N shell, first N shell, second B shell, first B shell, and total DOS.

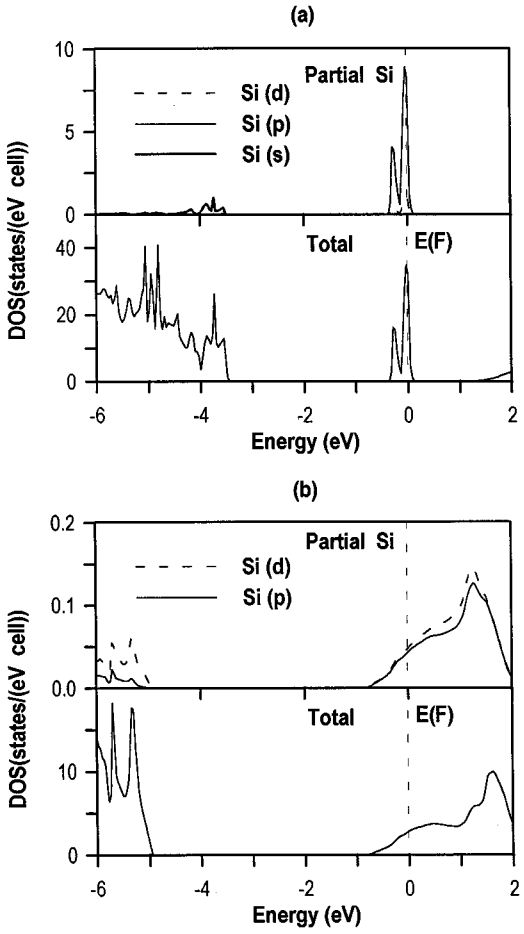

FIG. 9. s, p, and d orbital-projected densities of states for an isolated Si impurity at (a) a N site, and (b) a B site in c-BN. The total DOS is shown for comparison. (The s-type DOS for a Si impurity at a B site is an order of magnitude less than p- and d-type DOS's, and is not shown.)

curred at a value of b equal to 0.29, corresponding to a 1.82-Å Si-B bond length.

The latter case can be viewed similarly to those of Be and Mg substitutions for B: Si has one less electron than the N atom it replaces, and its bonding with the nearest B atoms is certainly weaker than an unperturbed B-N bond. The outward relaxation is also consistent with the large size of the Si atom, compared with the N atom for which it is substituted. The cause of the inward relaxation in the case of Si substituted for B is more subtle, however, and will be discussed later when we consider the charge distributions near the impurity site.

Figure 8 presents the total and shell-projected DOS for up to the fourth coordinational shell surrounding the Si impurity. A well-localized 0.33-eV-wide band occurs 1.29 eV below the conduction-band edge, with the Fermi level being found 0.96 eV below the conduction-band edge. These impurity states are hybridized with the $2p$ states of the nearest B atoms (the first B shell in Fig. 8), and, to a much smaller extent, with the $2p$ states of the N atoms of the next coordinational sphere (the first N shell). Negligible mixing occurs between the impurity level and atoms in more distant atomic shells. As is shown in Fig. 9, the impurity contribution is dominated by the $3p$ states of Si, with only a small d-state contribution being evident. The large 3.33-eV energy separation between the partially filled impurity band and the top of the valence band makes the transfer of electrons from the valence band impossible. It may be easier to excite an electron from the impurity band to the conduction band, even after accounting for the LDA underestimation of the band gap. The minimum-energy separation of twice the 0.96-eV Fermi-level separation to the conduction-band edge is still smaller than the 3.33-eV energy required to activate a hole. This large may account for the deep n-type level observed[8,25] in Si-doped c-BN, for which a 1.1-eV activation energy was measured,[25] the difference from the predicted values being attributable to the symmetric relaxation of the atoms nearest the impurity.

The strong localization of the impurity states is evident in Fig. 10(a), which shows the distribution of charges in the energy range from 0.5 eV to the Fermi level. The total-charge-density distribution in the (110) plane is shown in Fig. 10(b), where some covalency is evident in the Si-B bonding. The charge redistribution for Si replacing a N atom in c-BN are qualitatively similar to those shown previously for the c-BN:Mg system.

Although the N-substitutional Si impurities may introduce

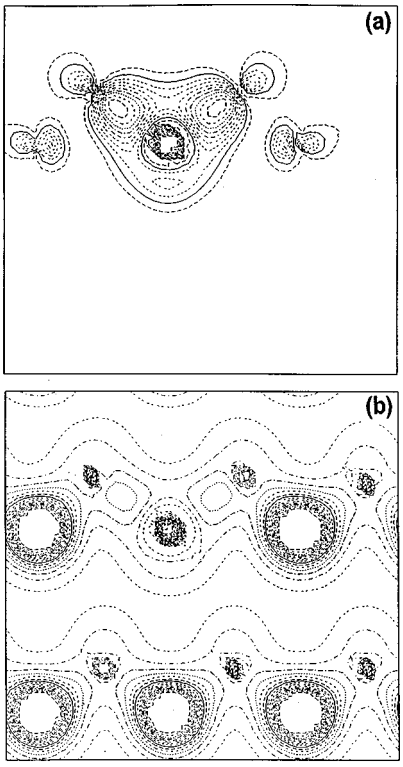

FIG. 10. Charge-density maps for c-BN with an isolated Si impurity at a N site. (a) (110)-plane charge density for the impurity-induced level. (b) (110)-plane total valence-band charge density.

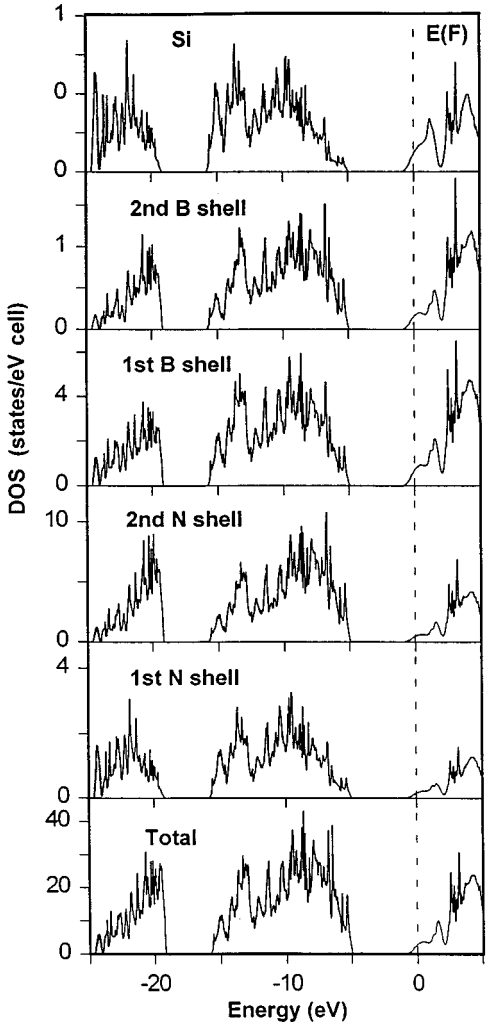

FIG. 11. Total and shell-projected DOS for an isolated Si impurity at a B site in c-BN: Si impurity, second B shell, first B shell, second N shell, first N shell, and total DOS.

only deep, n-type activation centers in c-BN, a completely different situation is predicted for Si substituted to the B sublattice. Our results for this type of impurity are presented in Figs. 11 and 12 and Table I. Figure 11 presents the total and shell-projected DOS for the lattice-relaxed 64-atom supercell with a Si atom substituted to the central B site. This configuration can contribute carriers to the conduction band of the host crystal, and exhibits a DOS of 2.80 states/(eV cell) at the Fermi level. There are two distinct features for this type of Si impurity: (i) the impurity does *not* form a sharp, localized donor level within the forbidden gap, and (ii) the states associated with the impurity itself hybridize extensively with the entire valence band of the host crystal, with somewhat greater contributions to the lower parts of s-type and p-type valence subbands (top panel, Fig. 11) than near the top of the valence band. The strong hybridization of the B-substitutional Si impurity is very much like the acceptor-type Be impurity considered in Sec. III. But the Si impurity has two electrons more than the Be atom. One of them fills the valence-band states, and the other contributes to the states in the conduction band, providing the n-type conductivity observed experimentally.[9]

As shown in Fig. 4(c), the main contributions of the impurity states to the conduction-band edge are from $3p$ orbitals of Si, with nearly as great a contribution being made by Si $3d$ states, due to relaxation. As in the case of the p-type doping associated with the Be impurity in c-BN, our calculations suggest that the traditional model of a localized donor impurity is not applicable for the n-type Si impurity states in c-BN.

Examination of the charges associated with the atomic spheres of atoms in different coordinational shells surrounding each impurity indicates that a greater accumulation of charge at the B-substitutional Si impurity than at the N-substitutional impurity. In the former case, most of the charge is shifted to the impurity from neighboring N atoms, so that they become less negative than in the ideal crystal. Due to the delocalized nature of the impurity states, however, the perturbation of the B-substitutional impurity is evident as far as the sixth coordinational shell. The (110)-plane charge-density map shown in Fig. 12 shows that the chemical bonding between the Si impurity and its neighbors is predominantly ionic, with the charge distributions of the N atoms in the first coordinational shell being strongly distorted toward the impurity. The effect of the inward relaxation of the first-N-shell atoms is clearly evident by comparing the charge-density distributions of the two atomic chains shown in Fig. 12(a). Figure 12(b) shows the corresponding charge-density contours for occupied impurity states in the conduction band having energies within 1.5 eV of the Fermi level. With appreciable charge density extending from the impurity to the second-nearest neighbors, the band-edge charge distribution clearly shows the highly delocalized character of the impurity-band carriers, particularly when

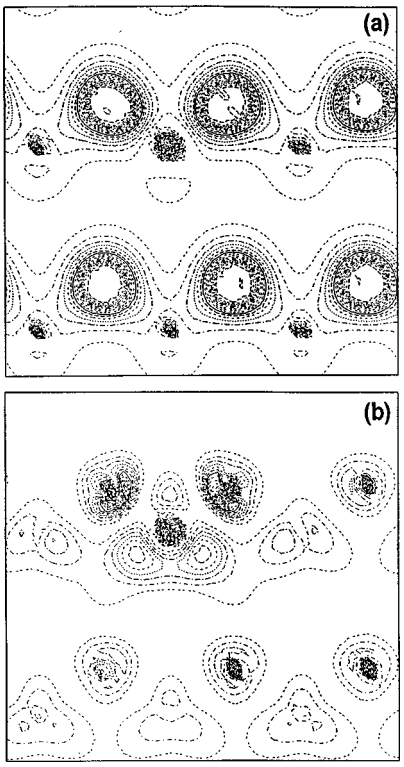

FIG. 12. Charge-density maps for c-BN with an isolated Si impurity substituted to the B sublattice. (a) (110)-plane charge density for occupied donor states in the conduction band. (b) (110)-plane total valence-band charge density.

compared with the corresponding N-substitutional-Si charge-density distribution shown in Fig. 10. The B-substitutional Si impurity tends to form metallic-type Si-B bonds with the atoms of the second coordinational sphere (first B shell). This illustrates that the isolated Si impurity, in substituting for a B atom in c-BN, acts as an efficient n-type donor, contributing highly delocalized electron states to the conduction-band edge.

V. SUMMARY

We have performed self-consistent TB-LMTO electronic-structure calculations for isolated Be, Mg, and Si impurities in zinc-blende BN. Using 64-atom supercells centered on the impurity site, we have investigated Be, Mg, and Si substituted to the B sublattice, and Si substituted to the N sublattice. For each of the impurities except Si substituted for N, the conventional model of pointlike impurities inducing narrow levels within the band gap was found to be inapplicable. The hole states of Be and Mg were merged to the valence-band edge, while the donor states of Si substituted for B overlapped with the conduction band of the c-BN host. A large outward relaxation was predicted for the atoms neighboring the Be and Mg impurities, as well as for the atoms nearest the N-substitutional Si impurity. A small inward relaxation was predicted in the vicinity of B-substitutional Si.

Both the Be and Mg impurities induce hole states at the valence-band edge. These states are responsible for the p-type conductivity in crystals doped with these impurities. Be-induced hole states appear to be strongly delocalized, consistent with the production of mobile p-type carriers in c-BN:Be. Mg-induced impurity states are significantly more localized, and appear to be less effective for p-type doping than Be-induced states.

A Si impurity substituted to the N sublattice forms narrow, localized, and partially occupied levels within the band gap, about 3.3 eV above the valence-band edge and 1.0 eV below the conduction-band edge. Electrons occupying these states may provide the n-type activated behavior in Si-doped c-BN crystals, for which a 1.1-eV activation energy has been measured.[25]

In contrast, a Si impurity substituted for a B atom in c-BN creates highly delocalized states that overlap the conduction-band edge. The extra electron of Si becomes efficiently delocalized over many atomic shells, and may result in n-type conductivity. Metallic Si-B bonds are formed, and can be clearly seen from charge-density maps. Participation of Si $3d$ states in the donorlike levels is noticeable due to the relaxation of the atoms nearest the impurity. These results explain the n-type conductivity exhibited in Si-doped BN crystals.[26]

The shell- and orbital-projected DOS and corresponding charge-density distributions provide detailed data regarding the electronic properties of isolated Be, Mg, and Si impurities in c-BN. The effective n- and p-type behavior shown in experiments can therefore be understood for the doped c-BN crystals.

ACKNOWLEDGMENTS

A grant of computer time on the Cray C-90 platform of the NSF San Diego Supercomputing Center is gratefully acknowledged.

[1] *Diamond, Silicon Carbide and Related Wide Bandgap Semiconductors*, edited by J. T. Glass, R. Messier, and N. Fujimori, MRS Symposia Proceedings No. 162 (Materials Research Society, Pittsburgh, 1990).

[2] J. H. Edgar, J. Mater. Res. **7**, 235 (1992).

[3] H. Saitoh, T. Hirose, H. Matsui, Y. Hirotsu, and Y. Ichinose, Surf. Coat. Technol. **39/40**, 265 (1989).

[4] T. Ikeda, Y. Kawate, and Y. Hirai, J. Vac. Sci. Technol. A **8**, 3168 (1990).

[5] M. Lu, A. Bousetta, R. Sukach, A. Bensaoula, K. Walters, K. Eipers-Smith, and A. Schultz, Appl. Phys. Lett. **64**, 1514 (1994).

[6] A. K. Ballal, L. Salamanca-Riba, G. L. Doll, C. A. Taylor, and R. Clarke, J. Mater. Res. **7**, 1618 (1992).

[7] D. J. Kester, K. S. Ailey, D. J. Lichtenwalner, and R. F. Davis, J. Vac. Sci. Technol. A **12**, 3074 (1994).

[8] O. Mishima, J. Tanaka, S. Yamaoka, and O. Fukunaga, Science **238**, 181 (1987).

[9] O. Mishima, K. Era, J. Tanaka, and S. Yamaoka, Appl. Phys. Lett. **53**, 962 (1988).

[10] D. J. Kester and R. Meissier, J. Appl. Phys. **72**, 504 (1992).
[11] L. J. Terminello, A. Chaiken, D. A. Lapiano-Smith, G. L. Doll, and T. Sato, J. Vac. Sci. Technol. A **12**, 2462 (1994).
[12] V. Cholet, L. Vandenbulcke, J. P. Rouan, P. Bailif, and R. Erre, J. Mater. Sci. **29**, 1417 (1994).
[13] N. E. Christensen and I. Gorczyga, Phys. Rev. B **50**, 4397 (1994).
[14] M. P. Surh, S. G. Louie, and M. Cohen, Phys. Rev. B **37**, 10 159 (1988).
[15] J. Furthmuller, J. Hafner, and G. Kresse, Phys. Rev. B **50**, 15 606 (1994).
[16] V. A. Gubanov, Z. W. Lu, B. M. Klein, and C. Y. Fong, Phys. Rev. B **53**, 4377 (1996).
[17] R. W. G. Wyskoff, *Crystal Structures*, 2nd ed. (Krieger, 1981); see also G. L. Doll, J. A. Sell, C. A. Taylor II, and R. Clarke, Phys. Rev. B **43**, 6816 (1991).
[18] D. J. Singh, *Planewaves, Pseudopotentials, and the LAPW Method* (Kluwer, Boston, 1994).
[19] M. Methfessel, Phys. Rev. B **38**, 1537 (1988).
[20] O. K. Andersen and O. Jepsen, Phys. Rev. Lett. **53**, 2571 (1984).
[21] V. Fiorentini, M. Methfessel, and M. Scheffler, Phys. Rev. B **47**, 13 353 (1993).
[22] F. Bernstedt and R. Del Sole, Phys. Rev. B **38**, 7710 (1988).
[23] L. Hedin and B. I. Lundquist, J. Phys. C **4**, 2064 (1971).
[24] M. van Schilfgaarde, T. A. Paxton, O. Jepsen, and O. K. Andersen, TB-LMTO Program-Version 44, Max Planck Institute for Solid State Physics, 1994.
[25] O. Mishima, S. Yamaoka, and O. Fukunaga, J. Appl. Phys. **61**, 2822 (1987).
[26] W. Faschinger, S. Ferreira, and H. Sitter, Appl. Phys. Lett. **66**, 2518 (1995).